ION–BEAM–INDUCED CRYSTALLIZATION AND AMORPHIZATION IN Zn^{+}–IMPLANTED SILICON

M. Kalitzova[a], R. A. Yankov[a*], S. Simov[a], Ch. Angelov[b], G. Vitali[c], C. Pizzuto[c], G. Zollo[c], D. Manno[d], J. Fauré[e], L. Kilian[e], P. Bonhomme[e]

[a]*G. Nadjakov Institute of Solid State Physics, Bulgarian Academy of Sciences, BG–1784 Sofia, Bulgaria,*
[b]*Institute of Nuclear Research and Nuclear Energy, Bulgarian Academy of Sciences, BG–1784 Sofia, Bulgaria,*
[c]*Dipartimento di Energetica, Universitá di Roma "La Sapienza", and INFM, Via A. Scarpa 14–00161 Roma, Italy,*
[d]*Dipartimento di Scienza dei Materiali and INFM, Universitá di Lecce, Via Arnesano, 73100 Lecce, Italy,*
[e]*Laboratoire de Microscopie Electronique, Université de Reims, INSERM U314 UFR Sciences, 21 Rue Clement Ader, 51100 Reims Cedex, France,*
[a]*<Markaliz@bgearn.acad.bg>*

(Received April 30, 1998)

The microstructural changes which occur during high–dose Zn^{+}– irradiation of (100) silicon have been studied. The implantations have been carried out at the energy of 50 keV using a beam current density of 10μA cm^{-2} and ion doses in the range of 1×10^{15} to 1×10^{18}cm^{-2}. Cross–sectional transmission electron microscopy in diffraction contrast and phase contrast modes has been employed in conjunction with other analytical techniques and computer simulations. The kinetics of the ion beam induced crystallization process has been examined as a function of implantation dose. A specific crystalline overlap has been observed in the near surface region influenced by the implantation, and this has been interpreted as formation of superlattices where Zn alternates Si along (111) direction. The experimental results have been discussed in terms of microscopic beam heating effects and the concept of critical dose ranges.

Key words: ion implantation, silicon, damage, amorphization, crystallization, XTEM.

PACS number(s): 61.16.–d, 61.72.Tt, 61.80.–x, 61.80.Jh

I. INTRODUCTION

It is well known that during the implantation of heavy ions at low energies (~100 keV) the interaction between the incident ions and the nuclei of the target atoms are the basic events that take place. As a result, collision cascades with high deposited energy density Θ_v develop in the crystal lattice and bring about a number of specific phenomena such as defect production, atomic mixing, formation of new metastable phases, amorphization etc. The accumulation of lattice damage up to complete amorphization in the near surface region is one of the most important effects in ion implanted semiconductor materials. When certain conditions are met, instead of growth, one can observe recrystallization of the amorphized layer. In most cases the process of ion–beam–induced crystallization (IBIC) has been studied during appropriate irradiation following the implantation which had generated disorder [1]. A similar phenomenon, often referred to as self–annealing or dynamic annealing, has been observed during implantation itself, typically at high beam current densities ($\geq 100\mu$ A cm^{-2}), [2,3]. It has also been shown that solid phase epitaxial crystallization induced by ion irradiation may occur at temperatures as low as 150^o C [4] instead of the standard solid phase epitaxial crystallization of amorphous (a)–layers in Si (necessitating temperatures >450^o C), and is characterized by an activation energy of ~0.2–0.3 eV [5]. Homogeneous nucleation of crystalline grains in an a–environment takes place at temperatures in excess of 600^o C with an activation energy of about 5 eV [6]. The dependence of the ion beam induced epitaxial crystallisation and planar amorphization of a–Si layers onto single–crystal Si substrates on the substrate temperature, the substrate orientation and the energy deposited by the incident ions have been discussed in details [7].

Recently, results pertinent to the IBIC process in a self–annealing regime during Zn^{+} ion implantation into single crystal Si at relatively low beam current densities ($\leq 10\mu$A/cm^{-2}) have been reported [8,9]. Transmission electron microscopy (TEM) analyses in diffraction contrast mode combined with other analytical techniques have been used to study recrystallized structures in an amorphized layer formed at doses $\leq 10^{17}$cm^{-2} whereby Si and Zn microcrystals and superpositions of nanocrystalline platelets of Zn and Si of different orientations have been identified.

The aim of the present work is to present a detailed characterization of the microstructure which develops during the processes of ion beam induced amorphization

*Present address: Institute of Ion Beam Physics and Materials Research, Research Centre Rossendorf, POB 510119, D–01314 Dresden, Germany

(IBIA) and IBIC under the above mentioned experimental conditions. In the course of these investigations, besides TEM in diffraction contrast, high resolution transmission electron microscopy (HRTEM) in phase contrast imaging mode has also been used. As is well known, HRTEM can provide a deeper and direct insight into the atomic structure of the materials studied [10,11].

II. SAMPLE PREPARATION AND EXPERIMENTAL TECHNIQUES FOR STRUCTURAL CHARACTERIZATION

In our experiments we used device grade, (100) oriented Si wafers of a thickness of 250–300 μm and resistivity of 17 Ω.cm. The wafers were implanted with 50 keV ions at an angle of 7^o with respect to the sample surface normal using a beam current density of 10μ A cm^{-2} and doses in the range of 1×10^{15} to $1\times10^{18}cm^{-2}$.

Recently the microstructure of 50 keV, high–dose Zn^+ implanted Si was studied by TEM in diffraction contrast and complementary information on the nature of the implantation induced damaged structures was obtained by x–ray energy dispersive analysis (EDAX) and reflection high energy electron diffraction (RHEED). The effects of sample heating, sputtering and diffusion as well as the evolution of the Zn concentration profiles as evaluated by Rutherford backscattering spectrometry (RBS) were taken into account, see [8, 9]. The present study is a sequel to this work and, by using HRTEM, sheds new light on the microstructure of the Zn^+ implanted Si under conditions favourable for IBIC and IBIA. Fourier filter processing of the experimentally obtained HRTEM images and multislice simulation of HRTEM images were also carried out. HRTEM microscopy was performed on cross–sectional specimens (XHRTEM). The $< 110 >$ cross–sections from (100) implanted Si samples were obtained by means of a technique similar to the one used in [12]. The final thinning was achieved by ion beam etching [13]. XHRTEM observations were made in a JEM 2010 electron microscope operating at an accelerating voltage of 160 KV. From selected areas of about 100 nm in diameter, small area electron diffraction (SAED) were taken with an approximately parallel electron beam (convergence angle about 5×10^{-5}rad) [14]. HRTEM images recorded with a LESA LH72LL–TEM camera were digitalized and processed.

III. RESULTS AND DISCUSSION

As our interest focuses on the processes of IBIA and IBIC in Zn^+ implanted single crystal Si, first an assessment of the amorphization dose ψ_a was made on the basis of the work reported in [15]. Specifically, a complete amorphization of the Si surface would occur at a dose of 3×10^{14} cm^{-2}. For this reason, the lowest ion dose used was taken to be 1×10^{15} cm^{-2}. The choice of the highest implant dose ($1\times10^{18}cm^{-2}$) was made on the basis of the threshold saturation Zn dose estimated for the case of the particular ion target combination used. The respective Zn profiles computed with the aid of a formula taken from [16] are shown in Fig. 1. According to the basic theory, saturation in the Zn depth distribution should be expected at doses above $2\times10^{17}cm^{-2}$. The Zn near surface concentration is about $2\times10^{22}cm^{-3}$ and hence for doses higher than $2\times10^{17}cm^{-2}$ the resulting depth distributions are expected to be identical. To ascertain the validity of these theoretical predictions, detailed RBS analysis was carried out the results of which are given elsewhere [9].

Fig. 2 shows the RUMP code [17] simulated Zn depth profiles based on the respective RBS data. Surprisingly, the RUMP simulation results reveal that the Zn concentration profile is far from saturation. It is evident that the peak of the unsaturated profile increases in height and moves to greater depths for higher doses. The retained doses as determined by RUMP prove to be 1×10^{16}, 2.4×10^{16} and $6.2\times10^{16}cm^{-2}$ which, if compared to the respective injected doses, implies that appreciable Zn removal from the near surface region together with Zn indiffusion must have occurred during implantation. Basically, three factors are believed to contribute to this behaviour: first, a large difference between the sputtering yields Y_s of Si and Zn, which are 2.5 and 25 at. ion^{-1}, respectively [8]; second, the low melting point of Zn (419.5^o C) which may have been reached in individual microregions as a consequence of local beam heating effects having in mind that the equilibrium substrate temperature in our experiments is assessed to be in the range 240–280^o C [8]; third , Zn exhibits fast diffusion in Si ($D_{Z_n} = 10^{-7}$–$10^{-6}cm^2s^{-1}$) [18]. Moreover, the diffusivity of Zn in Si would certainly be increased via radiation enhanced diffusion during implantation.

The changes in the microstructure of the implanted layers with increasing Zn^+ dose from $1\times10^{15}cm^{-2}$ to $1\times10^{18}cm^{-2}$ visualised by TEM in diffraction contrast, bright field (BF), are clearly seen in Fig. 3, a–e. For the two lower doses of 1×10^{15} and 1×10^{16} cm^{-2} (see Fig. 3, a and b) a crystalline to amorphous transformation was observed in the implanted layer. As can be seen, the contrast of the amorphized layers resulting from these two doses is much the same and is typical of homogeneous a–structures. What distinguishes them is the apparent decrease in the thickness of the a–layer formed at the higher dose of $1\times10^{16}cm^{-2}$ (610–630 Å) in comparison to that produced at $1\times10^{15}cm^{-2}$ (650–700 Å). The decrease is explained in terms of the a–c interface movement towards the surface during implantation as the dose is increased. The reverse–temperature (T_r) = 180^o C as calculated in [8] for the experimental conditions used in our case is reached and exceeded by the substrate temperature during implantation with $1\times10^{16}cm^{-2}$ for a difference of $1\times10^{15}cm^{-2}$. Accordingly, the process of IBIC is favoured for higher doses and the a–c interface moves toward the surface. It may be useful to point out that T_r is defined as that target temperature at which the processes of IBIA and IBIC are balanced and therefore no a–c interface movement would occur with increasing dose.

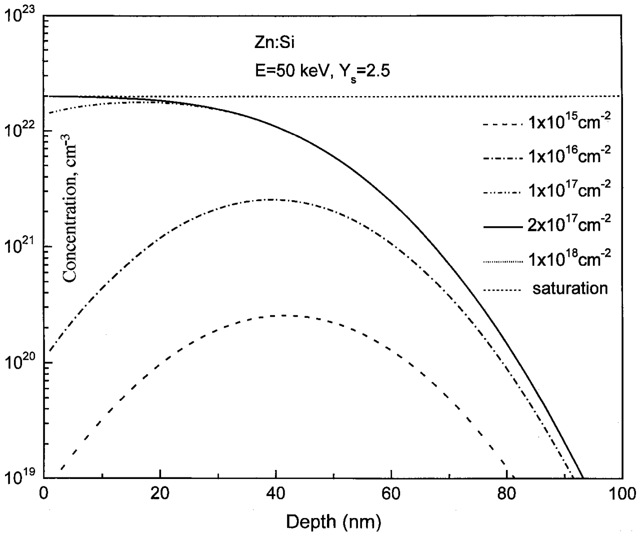

Fig. 1. Computed Zn concentration profiles of 50 keV Zn^{+} implanted in Si at doses: 1×10^{15}, 1×10^{16}, 1×10^{17} and $1\times10^{18}\,\mathrm{cm}^{-2}$. The conventional theory predicts saturation in the Zn depth distribution for doses above $2\times10^{17}\,\mathrm{cm}^{-2}$.

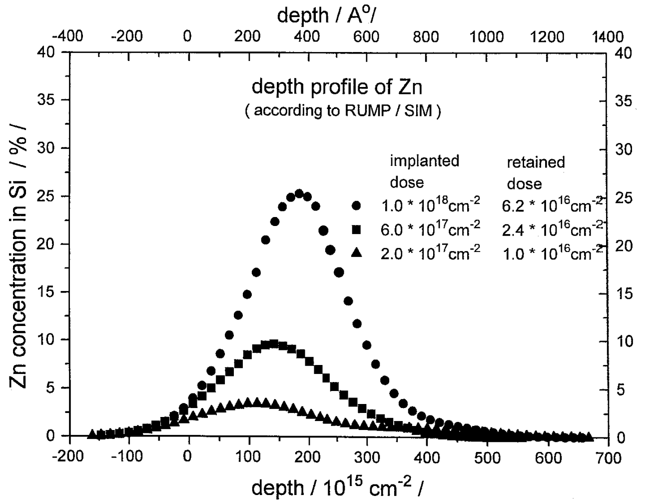

Fig. 2. Comparative plot of the simulated Zn profiles on the base of RBS spectra from 2×10^{17}, 6×10^{17} and $1\times10^{18}\,\mathrm{cm}^{-2}$ implants. The simulations are made by means of RUMP.

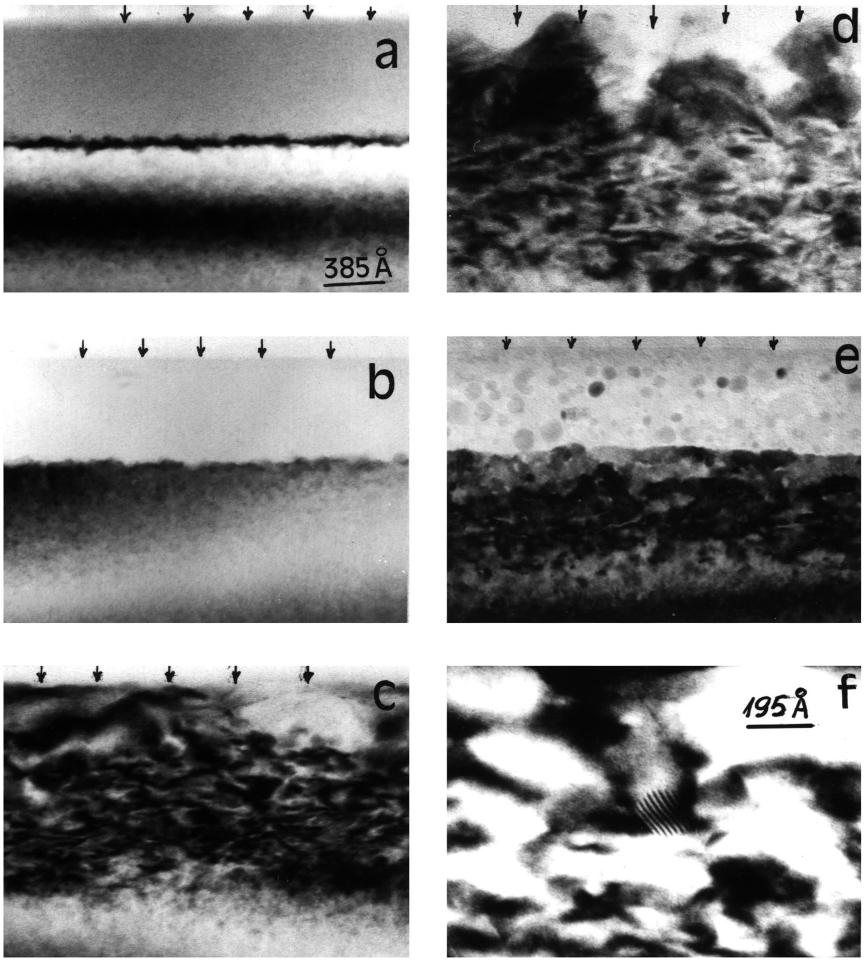

Fig. 3. XTEM bright–field images in (110) projection of 1×10^{15}(a), 1×10^{16}(b), 5×10^{16}(c), 1×10^{17}(d) and 1×10^{18}(e) implants. Moire fringes, observed in the damaged by the implantation at $5\times10^{16}\,\mathrm{cm}^{-2}$ layer, corresponding to overlapping of (200)Si and (10.0)Zn microcrystals (f).

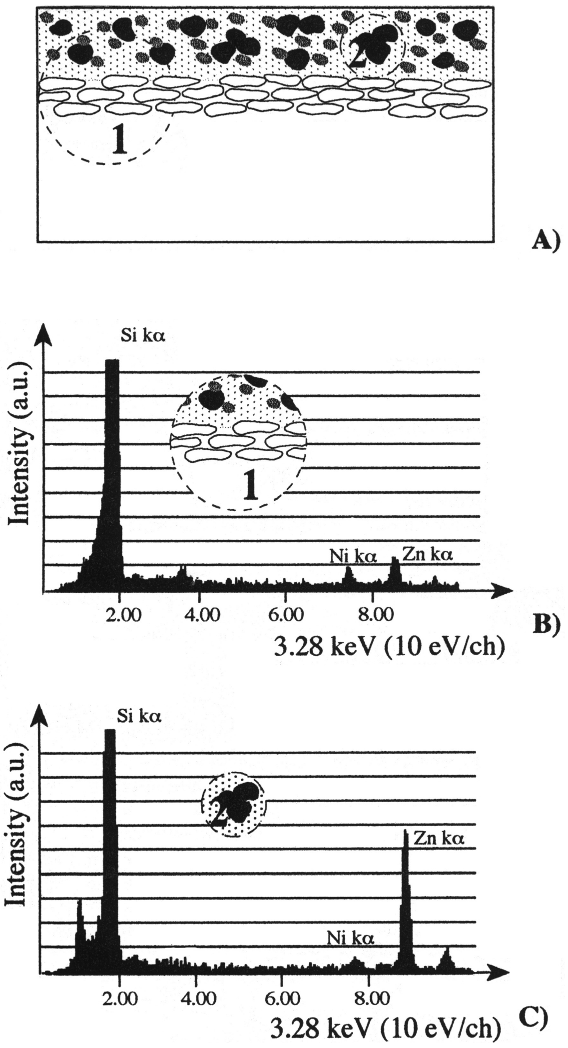

Fig. 4. EDAX spectra of different regions scanned over a cross–sectional specimen: (A) schematic representation of the XTEM micrograph in Fig. 3e, (B) region — type 1, (C) region — type 2.

At higher doses of 5×10^{16} and 1×10^{17}cm^{-2} the morphology of the implanted layer appears to be completely different, an a–to–c–transition is observed, see Fig. 3, c–d. The uniform a–layer resulting from the 1×10^{15} and 1×10^{16} cm^{-2} implants is transformed and characterized now by the formation of a complex microstructure consisting of mixed amorphous and crystalline phases. One can see in Fig. 3, f an example of the Moire fringes for a dose of 5×10^{16} cm^{-2} observed at higher magnification than that of the corresponding layer in Fig. 3, c. Comparing the microfotometric measurements of the respective fringe separations with calculations using the expressions for parallel Moire patterns [19] we identify the different Moire fringes as resulting from superpositions of differently oriented bulk Si and Zn nanocrystalline platelets. Especially the Moire fringes shown in Fig. 3, f are identified as resulting from superposition of (200)Si/(1010)Zn. For the case of 1×10^{17}cm^{-2} the surface roughness increases and the surface itself is partially eroded exhibiting distinct cone–like asperities. The thickness of the layer affected by the implants increases from 1100–1300 Å to 1300–2600 Å with increasing dose from 5×10^{16} to 1×10^{17}cm^{-2}. It should be noted that at such a high dose (1×10^{17}cm^{-2}) sputtering will have a profound effect on the surface topography as can be seen in Fig. 3, d. Specific surface erosion as well as preferential sputtering of Zn–rich areas (given the fact that Y_s of Zn bombarded with Zn^+ ions is about an order of magnitude higher than Y_s of Si bombarded with Zn^+) may contribute to the development of the cone–like asperities observed.

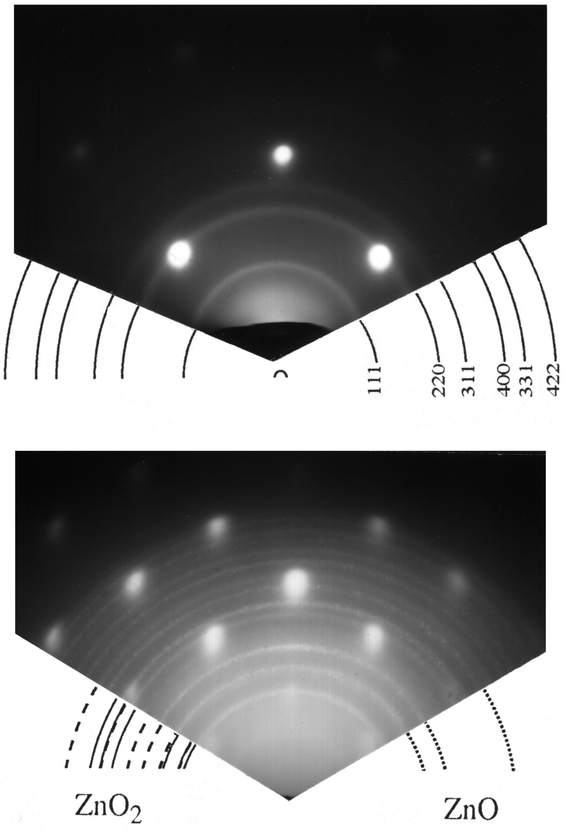

Fig. 5. RHEED patterns from the chemical etched for 5 h surface of sample implanted with 1×10^{18}cm^{-2}, $< 001 >$(a) and $< 011 >$(b) azimuth directions.

A new feature of the microstructure created by the highest doses used (above 1×10^{17}cm^{-2}) is the formation of a continuous amorphous layer in the upper part of the complex damage layer, incorporating microcrystalline clusters (in Fig. 3, e for a dose of 1×10^{18}cm^{-2} nanocrystalline clusters are seen with darker contrast, embedded in the uniform a–layer having lighter contrast). This a–layer extends to a depth of about 650 Å below the Si surface. Such a depth correlates with $R_p + 1.5\Delta R_p$, where

$R_p = 419\,\text{Å}$ is the projected range and $\Delta R_p = 156\,\text{Å}$ is the ion straggling. The formation of a different continuous a–layer at doses higher than $1{\times}10^{17}\text{cm}^{-2}$ might be explained by the nucleation of an a–phase due to the higher concentration of extended defects during the earlier stage of implantation (these extended defects are clearly seen in the case of the $1{\times}10^{17}\text{cm}^{-2}$ implant, Fig. 3, d). In the critical regime where the processes of dynamic annealing and defect production are balanced, the a–phase may be nucleated by the increased level of extended defects as has been established in [20]. EDAX microanalysis of this a–layer (see Fig. 4) containing microcrystal clusters reveals that the dark and grey regions seen in the continuous a–layer (Fig. 4, A, where the XTEM micrograph of Fig. 3, e, is schematically represented) are associated with Zn and Si microcrystals (Fig. 4, B and C).

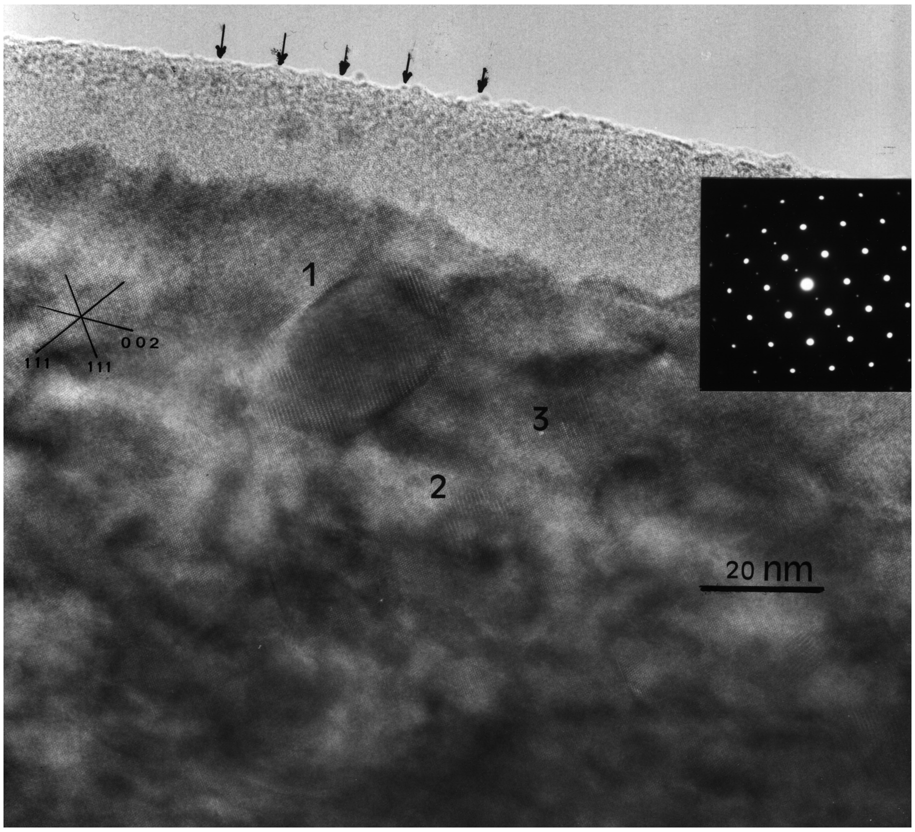

Fig. 6. XHRTEM imaging obtained in bright field mode with 7 reflexes in (110) projection of (100)Si, implanted at the dose of $5{\times}10^{16}\text{cm}^{-2}$; in the inset: SAED pattern from chosen area about 100 nm in diameter around regions 1,2 and 3.

This IBIC process occurring within the continuous a–layer formed at doses higher than $1{\times}10^{17}\text{cm}^{-2}$ is also demonstrated by the RHEED results. Fig. 5 shows RHEED patterns in (001) and (011) azimuth directions from the Si surface implanted with a dose of $1{\times}10^{18}\text{cm}^{-2}$ after chemical etching [9] for 5 hours. The analysis of the diffraction patterns shows that the rings arise from both Si (see Fig. 5, a) and mixture of polycrystalline Zn oxides (see Fig. 5, b). The presence of Zn oxide polycrystalline phases is attributed to the oxidation of Zn crystalline precipitates during chemical etching.

Fig. 6 shows XHRTEM lattice plane imaging obtained in bright field mode with 7 excited reflexes in (110) projection of (100) Si, implanted at dose of $5{\times}10^{16}\text{cm}^{-2}$. One can well distinguish the (111) and (002) planes of a crystalline Si layer strongly influenced by the Zn^{+} bombardment. In this damaged Si layer (compare with the Moire figure in Fig. 3) microcrystalline clusters are seen which have interplanar spaces different from those of Si (see regions, signed with 1, 2 and 3 in Fig. 6) and are positioned below the surface at a depth commensurate with R_p.

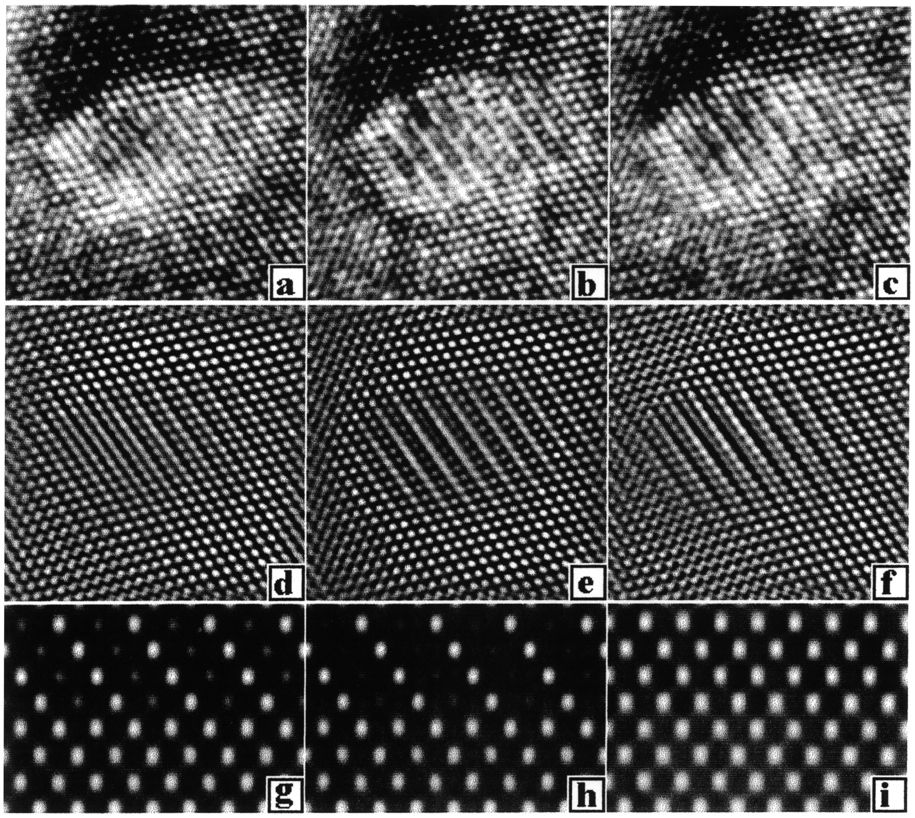

Fig. 7. HRTEM trough focus series of a typical overlapping crystal region: as acquired images (a–c), filtered images (d–f), and simulated ones (g–i), C_s=1.4 mm, and defocuses 50, 56 and 62 nm correspondingly.

A SAED pattern obtained from a selected area about 100 nm in diameter around region 1 in Fig. 6 is shown in the inset. Apart from the basic Si reflections in [110] projection, additional spots are evident in the SAED pattern. The interplanar spacing corresponding to the extra spots (smaller spots in the SAED pattern) does not fit the Zn spacings, and therefore it is impossible to interpret the second phase of crystalline inclusions seen in the XHRTEM image as Zn bulk nanocrystalline platelets overlapped with Si ones, similarly to the XTEM interpretation on the basis of Moire fringes. In order to remove the unwanted noise and enhance the structural features of the crystalline clusters, XHRTEM images have been processed by using an adaptive Fourier filter [21,22]. Fig. 7, a–c shows a trough focus series of as acquired image of a cluster similar to cluster 1 in Fig. 6. In Fig. 7, d–f the respective processed (filtered) XHRTEM images are shown. Taking into account the geometrical relation between the basic reflections of SAED in Fig. 6 arising from the Si matrix and the additional ones, we have interpreted the structure of the crystallites by simulating a superstructure where Zn alternates Si along the (111) direction. The simulation of HRTEM images is made in the multislice approach by using EMS packet software [23]. The simulated trough focus series obtained for a thickness of 20 nm, C_s=1.4 mm and defocus of 50, 56 and 62 nm is presented in Fig. 7, g–i and is in good agreement with the experimental images. In this way, by combining XTEM and XHRTEM we have been able to develop our understanding of the reason for the observed overlapping between the crystallized zones during IBIC over the dose range of 5×10^{16} to 1×10^{17}cm^{-2}. Fig. 8 shows the XHRTEM imaging of the microstructure of Zn^+ implanted Si surface for a dose of 1×10^{18}cm^{-2}. Once again it is evidenced (as shown by XTEM in diffraction contrast) that at the highest doses (2×10^{17}–1×10^{18}cm^{-2}) a continuous a–layer forms from the structured heavily damaged layer at lower doses (5×10^{16}–1×10^{17}cm^{-2}). Within this a–layer clusters of darker contrast are seen (Fig. 8). Some of them exhibit well expressed lattice plane fringes with distances corresponding to the Zn or Si interplanare spacings, as indicated in Fig. 8. One can notice in the XHRTEM images that the Zn crystallites are mainly present in a depth range around R_p ($\approx$ 420 A), corresponding exactly to the depth position of the crystal superlattice structures observed at a dose of 5×10^{16}cm^{-2}, while the Si crystalline nuclei are seen closer to the a–layer/crystalline matrix interface. In the inset to Fig. 8 the respective SAED pattern with diameter of the order of 100 nm is shown. Well expressed are the reflexes of the (110) zonal axis projection of the Si–matrix together with an a–Si halo near the central spot, and additional spots forming polycrystalline rings with radial distances from the central spot corresponding to 00.2, 10.0 and 10.1 interplanar spaces in the hexagonal Zn lattice (labelled a,b and c in the SAED pattern of Fig. 8).

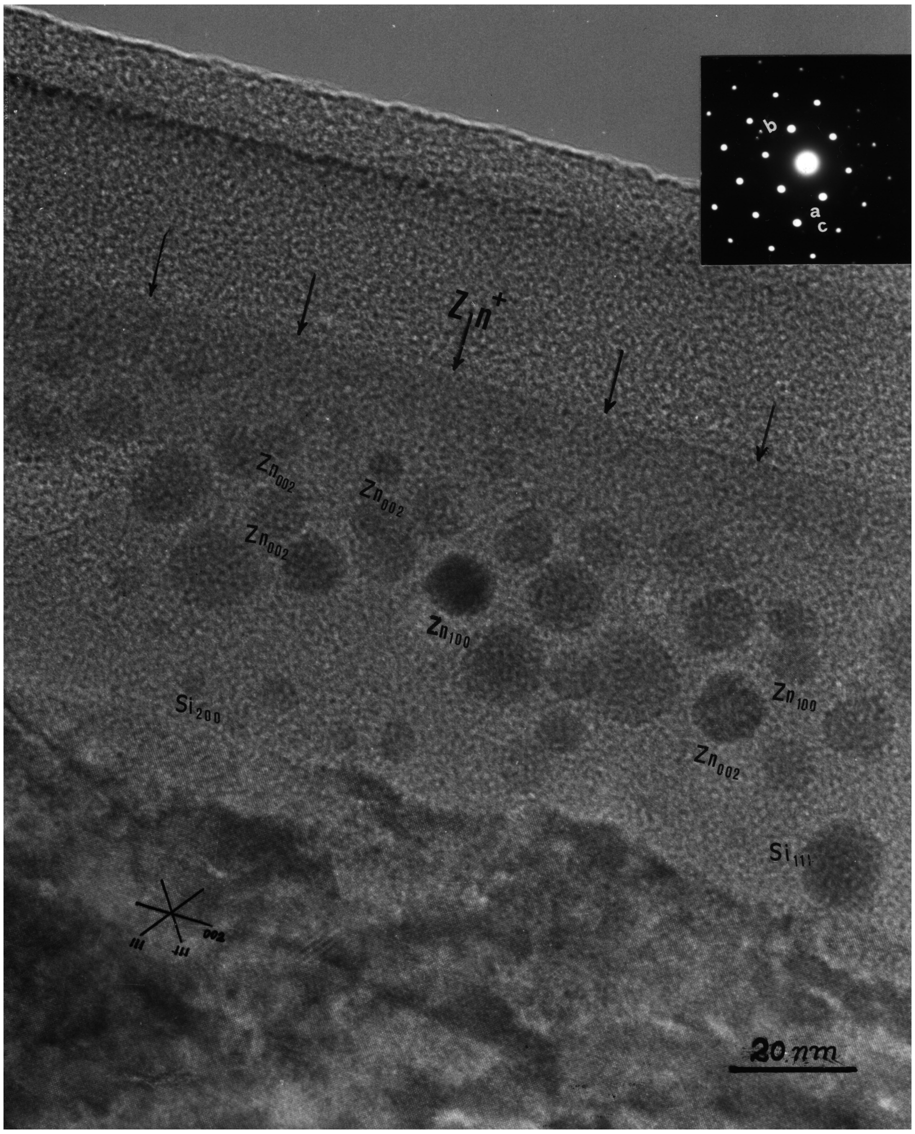

Fig. 8. XHRTEM imaging obtained in bright field mode with 7 reflexes in (110) projection of (100)Si, implanted at the dose of 1×10^{18}cm^{-2}; in the inset: SAED pattern from area brought from the amorphized Si–layer, with a, b and c are signed additional spots, corresponding to 00.2, 10.0 and 10.1 interplanar spaces of hexagonal Zn lattice.

IV. SUMMARY

The processes of ion beam induced crystallization and amorphization in Zn^{+} implanted Si have been studied. Cross–sectional transmission electron microscopy in diffraction contrast and phase contrast mode in combination with other analytical techniques and computer simulations have been used. The kinetics of the crystallization process as a function of the implant Zn dose has been examined. The results indicate that two critical dose ranges, namely 1×10^{16}–5×10^{16} and 1×10^{17}–2×10^{17} cm^{-2}, exist in which considerable structural changes occur in the Si/Zn system leading to complex c–to–a and a–

to–c phase transitions. For doses within the above specified ranges amorphization and/or crystallization may take place depending on the specific implant conditions. Small local fluctuations in the equilibrium substrate temperature may favour these two processes at relatively low beam current densities ($\approx 10\mu$A/cm^2) without any other external energetic influence.

The low solid solubility of Zn in Si (6×10^{16} cm^{-3}, [24]) and the high volume concentration ($\sim 10^{22}$ cm^{-3}) of Zn atoms at the maximum of the implant distribution imply that significant segregation of Zn atoms may take place at higher doses. It is important to note in this connection that for the binary eutectic Si–Zn the melting temperature is 419.3^o C [25], i.e. it is by only 0.2^o C lower than the melting point of Zn. It is reasonable to assume that in certain local regions of the Si matrix the temperature could rise to this level having in mind that the equilibrium value of the substrate temperature is $\sim 240^o$ C. In such regions Si + Zn nucleation could be initiated in situ at temperature much lower than those of the conventional solid–phase epitaxial regrowth. In this way it is possible to explain the formation of superlattice clusters of Si + Zn in the heavily damaged Si layer observed at a dose of 5×10^{16}cm^{-2} and depth $\approx R_p$. Increasing the doses above 1×10^{17}cm^{-2} leads to a second amorphization wave in the damaged layer. It might be that there is a specific memory effect during this process whereby some c–structures created at lower doses persist. In this way, it is possible to speculate that the superlattice structures grown at a dose of 5×10^{16}cm^{-2} act as nucleation sites for Zn nanocrystals.

ACKNOWLEDGMENTS

The authors are grateful to Professor N.Pashov for his helpful discussion and comments on the manuscript. This work was supported financially by the Italian CNR and Bulgarian National Science Foundation.

[1] J. Linnros, Ph.D. thesis, Chalmers University of Technology, Goteborg, Sweden (1985).
[2] G. F. Cembali, P. G. Merli, and F. Zignani, Appl. Phys. Lett. **38**, 808 (1981).
[3] F. F. Komarov, E. V. Kotov, A. P. Novikov, S. A. Petrov and V. I. Chitko, Radiat. Eff. **105**, 79 (1987).
[4] R. G. Elliman, J. S. Williams, W. L. Brown, A. Leiberich, D. M. Maher, and R. V. Knoell, Nucl. Instrum. Methods B **19/20**, 435 (1987).
[5] J. S. Williams, R. G. Elliman, W. L. Brown and T. E. Seidel, Phys. Rev. Lett. **55**, 1482 (1985).
[6] R. B. Iverson and R. Reif, J. Appl. Phys. **62**, 1675 (1987).
[7] F. Priolo and E. Rimini, Mat. Sci. Reports **5**, 321 (1990).
[8] S. Simov, M. Kalitzova, D. Karpuzov, R. Yankov, Ch. Angelov, J. Faure, P. Bonhomme and G. Balossier, J. Appl. Phys. **79**, 3470 (1996).
[9] M. Kalitzova, S. Simov, R. Yankov, Ch. Angelov, G. Vitali, M. Rossi, C. Pizzuto, G. Zollo, J. Faure, L. Killian, P. Bonhomme and M. Voelskow, J. Appl. Phys. **81**, 1143 (1997).
[10] J. M. Gibson, MRS Bull. XVI3 (1991).
[11] D. Van Dyck, Ultramicroscopy **55**, 99 (1994).
[12] T. T. Sheng and R. B. Markus, J. Electrochem. Soc. **127**, 737, (1980).
[13] L. M. Bharadwaj, J. Faure, P. Bonhomme and G. Balossier, Microsc. Microanal. Microstruct. **2**, 89 (1991).
[14] M. Tanaka, M. Terauchi, T. Kaneyama, in *Convergent Beam Electron Diffraction II* (Jeol LTD, Tokyo, 1987).
[15] A. B. Danilin and V. N. Mordkovich, Appl. Phys. Lett. **59**, 1570 (1991).
[16] H. Ryssel and J. Rude, *Ionenimplantation* (Tuebner, Stuttgart, 1987), p.p. 78, 79.
[17] L. R. Doolite, Nucl. Instrum. Methods Phys. Res. B **9**, 344 (1985).
[18] E. R. Weber, Appl. Phys. A **30**, 1 (1983).
[19] *Practical Electron Microscopy in Material Science*, edited by J. W. Edington (Van Nostrand Reinhold, N.Y. 1975), Section 3, p. 190.
[20] J. S. Williams, H. H. Tau, R. D. Goldberg, R. A. Brown, and C. Jagadish, in *Proceedings of MRS Symposium Fall Meeting.Materials Synthesis and Processings Using Ion Beams, Boston, MA, 1994* (MRS, Pitsburg, PA, 1994), p. 15.
[21] A. F. De Jong, W. Coene and D. Van Dyck, Ultramicroscopy **27**, 53 (1989).
[22] G. Mobus, G. Necker, M. Ruhle, Ultramicroscopy **49**, 46 (1993).
[23] P. A. Stadelman, Ultramicroscopy **21**, 131 (1987).
[24] A. G. Milnes, *Deep Impurities in Semiconductors* (Wiley, New York), p. 38, [Translated into Russian (Mir, Moskow, 1977)].
[25] R. P. Elliot, *Constitution of Binary Alloys, First Supplement vol. 2,* (Mc Graw–Hill, New York), p. 419, [Translated into Russian (Metalurgiia, Moscow, 1970)].